Automated Detection of Standard Image Planes in 3D Echocardiographic Images

Wei Peng[1], XiaoPing Liu[2(✉)], and Lanping Wu[3]

[1] Information Technology Support, East China Normal University, Shanghai 200062, China
wpeng@admin.ecnu.edu.cn
[2] Computer Center, East China Normal University, Shanghai 200062, China
xpliu@cc.ecnu.edu.cn
[3] Shanghai Children's Medical Center, Shanghai Jiaotong University, Shanghai 200240, China

Abstract. During the diagnosis and analysis of complex congenital heart malformation, it is time-consuming and tedious for doctors to search for standard image planes by hand from among the huge amounts of patients' three-dimensional (3D) ultrasound heart images. To relieve the laborious manual searching task for echocardiographers, especially for non-physicians, this paper focuses on the auto-detection of five standard image planes suggested by experts in the 3D echocardiographic images. Firstly, the four-chamber (4C) image plane is auto-detected by template matching, and then the other standard image planes are obtained according to their spatial relation with the 4C image plane. We have tested our methods on 28 normal and 22 abnormal datasets, and the error rates are 7.1% and 13.6%, respectively. With low computational complexity and simple operation, the method of auto-detection of standard planes in 3D echocardiographic images shows encouraging prospects of application.

Keywords: 3D ultrasound image · 3D echocardiographic image · Template matching · Image retrieval

1 Introduction

The congenital heart disease (CHD) is a group of cardiac anomalies in a three-dimensional (3D) space. Its diagnosis is always a difficult problem in cardiology. Today, real-time 3D echocardiography (RT3DE) [1–3] has become an important tool to diagnose CHD. With RT3DE, you can see a beating heart and choose any cross section to observe the internal structure of the heart. To facilitate the diagnosis of complex congenital heart malformation, five standard image planes (SIP) [4] are used in both research and clinical practice [5–7]. They are the long-axis planes of left and right ventricular (L1, L2), the short axis planes of atria and ventricular (S1, S2) and the four-chamber plane (H), as shown in Fig. 1. However, it is time-consuming and boring for doctors to manually search standard image planes with RT3DE systems or off-line software. Automatic detection of SIP in 3D echocardiographic (3DE) images will relieve the laborious

H. Gao et al. (Eds.): CollaborateCom 2020, LNICST 350, pp. 386–395, 2021.
https://doi.org/10.1007/978-3-030-67540-0_23

manual searching for echocardiographers, especially for non-physicians. In addition, it can be a prior process for 3DE image registration, fusion, analysis, etc., and can help non-physicians with rapid processing for research purposes.

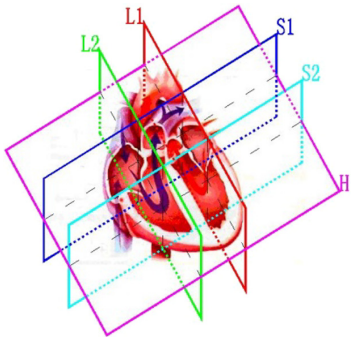

Fig. 1. Diagram of the five standard image planes (SIP) to visualize the heart.

3DE images are usually acquired from multiple different locations, and the image content thus obtained in different location is distinct. The image acquired at the left apical, which is called the apical dataset, is most commonly used in assessing the mitral or tricuspid valve disease and atrioventricular septal defects, and in measuring left ventricular parameters. As an initial work, this paper focuses on the detection of the five SIPs in the apical datasets.

The main innovations of this paper are as follows:

- Since few investigations on the problem have been reported at home and abroad, the automatic detection of the best cross-sections in 3-D echocardiac image is essential and valuable.
- As a preliminary work, we retrieve the 4C plane from the cross-sections extracted from the 3-D volume data with a 4C plane template, referring to the doctor's knowledge. Subsequently, the other best cross-sections could be detected, according to their spatial relation with the 4C plane.
- A coarse-to-fine approach is applied to retrieve the 4C plane with inspiring experimental results.

2 Related Work

Previous work closely related to our study includes techniques to distinguish the 4C image. Zhou et al. presented a method to differentiate between the apical 2C and 4C views, and it requires a pre-processing phase in which the left ventricle is identified by human [8]. To recognize the 4C image automatically, the number of horizontal and vertical borders in the image was used in [9]. With an intensity-based rigid registration method, Leung et al. registered the 3DE data set acquired in the stress stage, the data in the rest stage had already manually selected the two-dimensional (2D) planes

as reference, and they detected the two-chamber (2C), 4C and short-axis planes [10]. However, the computational complexity for registration of ultrasound volume is high and it is troublesome to perform 3DE image registration for different subjects.

All the above papers have discussed the detection of the 4C image from enormous 2D echocardiographic (2DE) images. Inspired by these methods, we attempt to detect the 4C image plane in the apical dataset with a template matching based method. Then we try to obtain the other planes according to their spatial relation with the 4C plane.

3 Materials and Methods

3.1 Apical 3DE Datasets

To detect the SIPs in the apical dataset, we should first study the structure of these datasets. An apical dataset is composed of a sequence of volume data. An end-diastolic volume data is shown in Fig. 2. As shown in Fig. 2, each volume data includes the original ultrasound acquisition data shaped approximately like a pyramid and the background data. The pyramid's azimuth and elevation angular spans is 60°. And the values of the black background voxels are zero. Since the four-chamber view in the end-diastolic data is the easiest to identify, we have extracted the end-diastolic volume data from the apical dataset. According to the characteristic of the end-diastolic volume data shown in Fig. 2, we assume that the pyramid apex is the left apex of the heart, and the central axis passing through the cube data is the long axis of the heart. Based on these assumptions, we have established a coordinate system as shown in Fig. 3. We set the pyramid apex to the origin O of the coordinate system, and the central axis OZ passes through the origin O, as shown in Fig. 3. In this way, a 4C cross-section can be found in a series of cross-sections that rotate about the axis OZ.

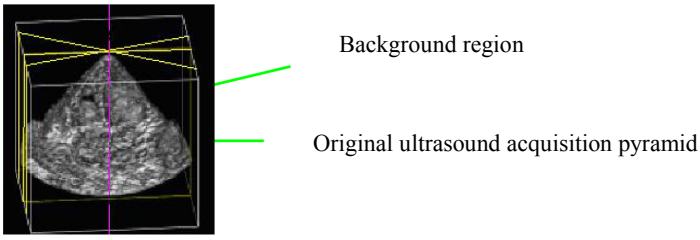

Fig. 2. The 3DE image of the end-diastolic volume data

3.2 Four-Chamber Image Detection

To find the 4C image plane in the 3D volume by template matching, we take the following steps. Firstly, a 4C image plane in the end-diastolic volume data of a normal person is selected as the template image. Secondly, a series of cross sections around the central axis are extracted from the end-diastolic volume data of an apical dataset. Thus an image library composed of these cross-sections is established. In the third step, by a coarse-to-fine strategy, the image most similar to the template image is retrieved from the image library, which is considered to be the 4C image plane.

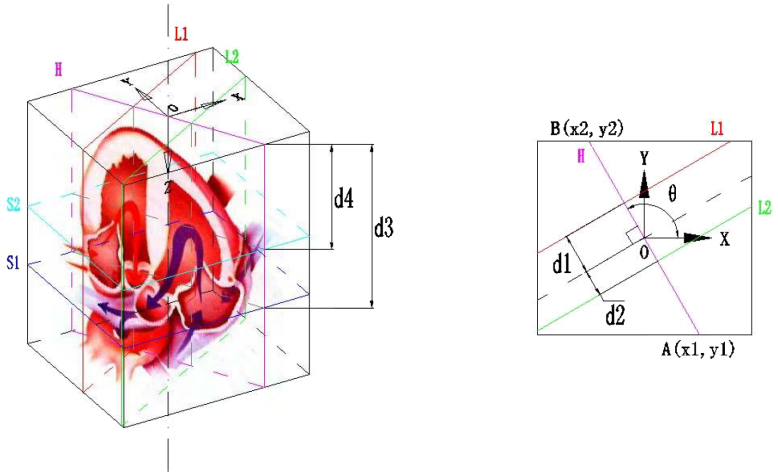

(a) (b)

Fig. 3. Diagram of the location of the heart and its five SIPs in the 3D coordinate system of the apical dataset. (a) Diagram of the heart and its five SIPs in the 3D coordinate system. (b) Diagram of the projection of the long axis of L1 and L2 in the XOY plane.

3.2.1 Template Selection

The commonly used simple template matching method is difficult to apply to echocardiographic images. Due to changes of the size and shape of the heart, deviation of the positions to collect data, differences of the ultrasound image intensities, and the multiple deformities in the congenital heart disease, it is necessary to build a big template library, which will lead to a high computational cost. Schlomo et al. match the unknown sample image onto known templates by a multi-scale elastic registration using only one or very few templates to identify the 4C image [12].

In our research, we choose a rectangular area from the center of the 4C cross-section of a normal end-diastolic data as the template image, which is described in Fig. 4. The characteristics of the septum and the chamber in the rectangular region of the end-diastolic four-chamber view are obvious, which is significantly different from the distribution of other image planes, and the feature is almost independent of the size, shape and image intensity of the heart, etc. Consequently, it is feasible to detect the most similar 4C image without a large template library. Furthermore, it saves time compared with matching the 4C image by elastic registration since a 3D dataset contains hundreds of 2D images.

3.2.2 Image Library Establishment

An image library is created by extracting a series of cross-sections from the 3D end-diastolic volume data. According to the coordinate system established in Fig. 3, this series of cross-sections share a common central axis OZ, and the projection of any

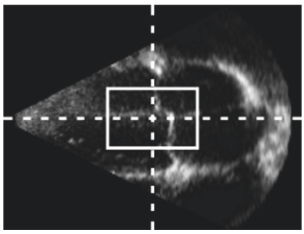

Fig. 4. Diagram of the central rectangular area in the apical 4C image

cross-section on the XOY plane is a line such as AB shown in Fig. 3(b). The coordinates of the point P on a certain cross-section satisfy Eq. 1:

$$\begin{cases} x = x1 + l\ \cos\theta \\ y = y1 + l\ \sin\theta \end{cases} (0^\circ \leq \theta \leq 180^\circ) \tag{1}$$

In Eq. 1, θ represents the included angle between line AB and the positive axis OX, ranging from 0 to 179, as shown in Fig. 3(b). And l denotes the Euler distance from the projection of point P on the XOY plane to point A, along the direction of line AB. l is smaller than or equal to L. L is the length of line AB, and is also the width of the cross section, which is defined as:

$$L = \overline{AB} = \sqrt{(x2 - x1)^2 + (y2 - y1)^2} \tag{2}$$

In Eq. 2, the coordinates of point A and point B are ($x1$, $y1$) and ($x2$, $y2$), respectively. In Fig. 3, the ordinate value of the boundary point A, $y1$, can be calculated by the distance from the origin O to the boundary line of the volumetric data passing through point A. And the abscissa of point A, $x1$ can be calculated by the product of the value of $y1$ and the tangent function value of θ.

In this way, according to angle θ (ranging from 0 to 179), cross-sections are extracted per degree, and a total of 180 slices are obtained to form an image library. The size of each slice is $L \times n$, and n is the size of the volume data in the OZ direction. In the paper, the units of the sizes are pixels.

3.2.3 4C Image Retrieval

A coarse-to-fine strategy is utilized in the 4C image retrieval. Due to the high speckle-noise, non-constant intensities and discontinuous structural edges, it is infeasible to segment the septum of the heart from the echocardiographic images. The coarse-to-fine strategy improves the speed and accuracy of the 4C image retrieval.

Firstly, to reduce the index size and retrieval time, a coarse retrieval is implemented. Due to the movement of the probe and patient respiration, the heart septum tissue will inevitably offset from its ideal position. As a transformation, rotation and scale invariant feature, image histogram is relatively robust to the misalignment. We adopt the cumulative histogram of the rectangular region as the feature. As shown in Fig. 3, the geometric

center of this region is the same as that of the cross section. Given two images G and S, their dissimilarity measure is defined as

$$dissim(G, S) = \sum_{i=0}^{255} |g(i) - s(i)| \tag{3}$$

Here, i is the image intensity ranging from 0 to 255. $g(i)$ and $s(i)$ are cumulative histograms of G and S, respectively. $g(i)$ is defined as:

$$g(i) = \sum_{k=0}^{i} \frac{n_k}{N} \tag{4}$$

in which, N is the total number of the pixels of the image. n_k is the number of the pixels whose intensity values are equal to k. *dissim (G, S)* is set to zero if two images are identical.

Next, in order to eliminate the misalignment error, we apply a rigid registration method to match the optimal rectangular area in each cross-section image of the decreased image set preprocessed by the coarse retrieval. Before the fine search, we take the cross-correlation of the two images as the similarity measure, and use the simplex algorithm [13] as the optimization strategy to achieve the optimal match. As a result, the sensitive factors of scale, transformation and rotation changes of the wavelet feature in the fine retrieval are deleted to have good results.

Finally, the fine retrieval is implemented by catching the difference between the template image and the best matches of the images of the reduced image set. Since the wavelet transform has a multi-resolution property, the image transformed by wavelet can be indexed in a hierarchical form [14]. We can extract direction information from sub-bands in various directions to improve index performance [15]. The Daubechies wavelets [16], based on the work of Ingrid Daubechies, are a family of orthogonal wavelets defining a discrete wavelet transformation and characterized by a maximal number of vanishing moments for some given support. In order to detect the local detailed information of the rectangular area image, we perform wavelet transformation on the image by the wavelet function db2 and decompose the image into four sub-bands, LL1, HL1, HV1 and HD1. We calculate the mean E and variance V of the wavelet coefficients of the three high frequency sub-bands, HL1, HV1 and HD1. E and V are respectively defined by Eq. 5 and Eq. 6.

$$E = \frac{1}{MN} \sum_{m=1}^{M} \sum_{n=1}^{N} |x(m, n)| \tag{5}$$

$$V = \frac{1}{MN} \sum_{m=1}^{M} \sum_{n=1}^{N} \left| x(m, n)^2 - E^2 \right| \tag{6}$$

In Eq. 5 and Eq. 6, the sizes of the sub-bands are M by N. Here, x is the wavelet coefficient matrix of the high-frequency sub-bands. We design $\vec{f}$ (EHL1, VHL1, EHV1, VHV1, EHD1, VHD1) as the feature vector of the image. The dissimilarity of two images is measured by the Euclidean distance of $\vec{f}$. Finally, the image with the minimum Euclidean distance is detected as a 4C image.

3.3 Other Planes' Detection

According to Fig. 3, the other SIPs including L1, L2, S1 and S2 could be assumed perpendicular to the 4C image plane, H. The distance from L1, L2, S1 and S2 to the origin, point O, is respectively d1, d2, d3 and d4 as shown in Fig. 3. If the coordinate (x, y, z) of point P can satisfy any of the following Eq. 7, 8, 9 or 10, point P is located on the corresponding planes L1, L2, L3 or L4.

$$\text{L1: } x\cos\theta + y\sin\theta = d1 \tag{7}$$

$$\text{L2: } x\cos\theta + y\sin\theta = -d2 \tag{8}$$

$$\text{S1: } z = d3 \tag{9}$$

$$\text{S2: } z = d4 \tag{10}$$

The positions of the standard image planes should not be thought of as single and precisely fixed. They are approximate and flexible. Though the heart size of a 3DE image usually ranges approximately from 0.7 to 1.3 times the size in the template 3DE image, d1, d2, d3 and d4 could be equal to those in the template 3D volume which are pre-defined.

4 Experimental Results

The experimental datasets used in our study were the full-volume data collected by Philips Sonos 7500. The experimental data included 28 normal and 22 abnormal full-volume data. At different time, the normal datasets were collected from 16 normal children aged from 1 month and 12 years old, and the abnormal datasets were collected from 14 patients aged from 3 months to 13 years old. Figure 5 lists the detected 4C images of the 28 normal and 22 abnormal datasets.

To further quantitatively analyze our experimental results, we use the angle θ in Fig. 3 to indicate the position of the four-chamber section. Since the 4C image plane is not precisely fixed at a certain position, image planes located nearby may also be regarded as a 4C image. Therefore, image planes with a value of angle θ within a reasonable range can also be considered as valid 4C image plane.

Firstly, we asked three experienced sonographers to manually search the valid 4C image planes in each individual data. Each 4C image plane is quantified by θ. The image plane with a value of θ equal to the average values of θ of all the 4C image planes is considered to be the reference 4C image plane. To determine a reasonable range of the value of θ, a 4C image planes' library is established, which includes image planes from all datasets with d ranging from 0 to 20. d is defined as the absolute angular deviation from the reference 4C image plane. After checking all the images in the 4C image planes' library, $d \leq 10°$ was chosen to be a reliable range of the valid 4C cross section since the echocardiographers were 99% confident that the 4C image planes in this range should be accepted.

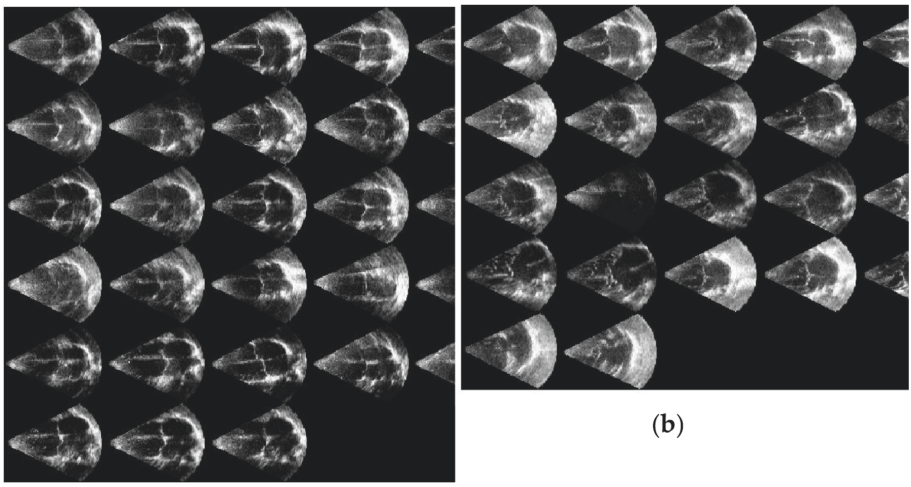

(a) (b)

Fig. 5. Experimental result of the detected 4c image in 3-DE images; (a) Experimental results of 28 normal data; (b) Experimental results of 22 abnormal data.

Table 1 lists the error rates with different ranges of d. As shown in Table 1, with d ranged from 8 to 10°, the correct rates of our method are 93% for 28 normal datasets and 91% for 22 CAVC datasets, which are acceptable in clinical applications. However, the results are still affected by factors such as image noise, etc. For example, we find in the experiment that the template image with lower speckle noise can obtain a higher accuracy rate than a blurred template image.

Table 1. Error rates list with different scope of d

d	Error rates of normal datasets	Error rates of CAVC datasets
0–3	32%	36%
3–6	25%	18%
6–8	7%	14%
8–10	7%	9%
>10	4%	9%

We compared this coarse-to-fine algorithm with the 3d rigid registration method [16] on the same computer and get the correct rates of the 4C image plane as listed in Table 2.

With the detected 4C image plane, the other standard image planes can be found by Eq. 7–10. Figure 6 lists examples of the detected standard image planes of a normal and an abnormal datasets, respectively.

Table 2. List of the correct rate of the two methods

Method	Correct rate	
	Normal datasets	CAVC datasets
Coarse-to-fine method	93%	91%
3d rigid registration method	85%	52%

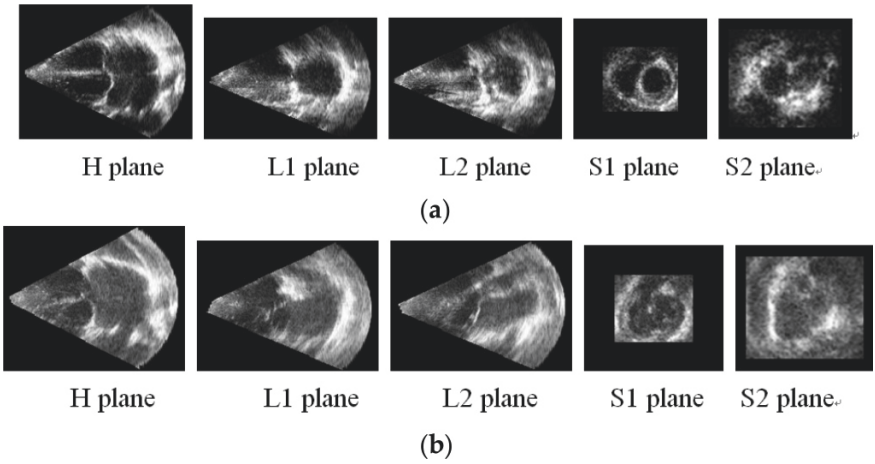

Fig. 6. The detected standard images in 3-DE images; (a) 5 standard images in a normal data; (b) 5 standard images in an abnormal data.

5 Conclusions

We detect the 4C image plane with a template matching method, and the other four SIPs L1, L2, S1 and S2 according to their positional relationship with each other. The accuracy of the detection of the 4C image plane is critically important. In order to improve the accuracy, we adopt a coarse to fine retrieval strategy. During our experiments, we find that a clear and high-quality template image improves the accuracy of our algorithm. Currently, our method only applies to the dataset collected by the left apex. How to extract the SIPs in the 3DE images collected in other positions is an important issue to be solved in our future research.

References

1. Adriaanse, B.M.E., van Vugt, J.M.G., Haak, M.C.: Three- and four-dimensional ultrasound in fetal echocardiography: an up-to-date overview. J. Perinatol. **36**(9), 685–693 (2016)
2. Dave, J.K., Mc Donald, M.E., Mehrotra, P., Kohut, A.R., Eisenbrey, J.R., Forsberg, F.: Recent technological advancements in cardiac ultrasound imaging. Ultrasonics **84**, 329–340 (2018)
3. Joao, P., Daniel, B., Nuno, A., Olivier, B., Johan, B., Jan, D.: Cardiac chamber volumetric assessment using 3D ultrasound - a review. Curr. Pharm. Des. **22**(1), 105–121 (2016)

4. Sun, K., Chen, S., Jiang, H.: A methodological study on three-dimensional echocardiographic sectional diagnosis for complex congenital heart malformation. Zhongguo Chaosheng Yixue Zazhi **15**(2), 84–88 (1999)
5. Zhou, J., et al.: Clinical value of fetal intelligent navigation echocardiography (5D Heart) in the display of key diagnostic elements in basic fetal echocardiographic views. Chin. J. Ultrason. **26**(7), 592–598 (2017)
6. Li, J.: 3D Visualization and Computer Aided Diagnosis Based on Heart Images. Shanghai Jiaotong University, Shanghai (2015)
7. Chen, G.: Methodological Study and Application of Real-Time Three-Dimensional Echocardiography in Children with Complex Congenital Heart Disease. Fudan University, Shanghai (2006)
8. Zhou, S.K., Park, J., Georgescu, B., Comaniciu, D., Simopoulos, C., Otsuki, J.: Image-based multiclass boosting and echocardiographic view classification. In: Proceedings of the 2006 IEEE Computer Society Conference on Computer Vision and Pattern Recognition, vol. 2, pp. 1559–1565 (2006)
9. Otey, M.E., et al.: Automatic view recognition for cardiac ultrasound images. In: Proceedings of the 1st International Workshop on Computer Vision for Intravascular and Intracardiac Imaging at Annual Conference on Medical Image Computing and Computer-Assisted Intervention (2008)
10. Leung, K.Y.E., et al.: Proceedings of the SPIE (2006)
11. Xiaoping, L., Xin, Y., Lanping, W., Xiao, T.: 2010 International Conference on Bioinformatics and Biomedical Technology (2010)
12. Aschkenasy, S.V., et al.: Unsupervised image classification of medical ultrasound data by multiresolution elastic registration. Ultrasound Med. Biol. **32**(7), 1047–1054 (2006)
13. Lagarias, J.C., Reeds, J.A., Wright, M.H., Wright, P.E.: Convergence properties of the Nelder-Mead simplex method in low dimensions. SIAM J. Optim. **9**(1), 112–147 (1998)
14. Mandal, M.K., Aboulnasr, T., Panchanathan, S.: Fast wavelet histogram techniques for image indexing. Comput. Vis. Image Underst. **75**(1–2), 99–110 (1999)
15. Laine, A., Fan, J.: Texture classification by wavelet packet signatures. IEEE Trans. Pattern Anal. Mach. Intell. **15**(11), 1186–1191 (1993)
16. Daubechies, I.: The wavelet transform, time-frequency localization and signal analysis. IEEE Trans. Inf. Theory **36**(5), 961–1005 (1990)